ELSEVIER

A REVIEW OF MRI PULSE SEQUENCES AND TECHNIQUES IN NEUROIMAGING

Edward F. Jackson, Ph.D., Lawrence E. Ginsberg, M.D., Don F. Schomer, M.D., and Norman E. Leeds, M.D.
Department of Diagnostic Radiology, The University of Texas M.D. Anderson Cancer Center, Houston, Texas

Jackson EF, Ginsberg LE, Schomer DF, Leeds NE. A review of MRI pulse sequences and techniques in neuroimaging. Surg Neurol 1997;47:185–99.

BACKGROUND
The unmatched soft tissue contrast provided by magnetic resonance imaging (MRI) has made it the modality of choice for many neuroimaging examinations. The fact that signal intensity in MRI depends on many parameters, including spin–lattice and spin–spin relaxation times, proton density, and velocity, makes it possible to highlight various pathologies by appropriate choice of pulse sequences and pulse sequence parameters. It is somewhat overwhelming, however, to filter through various pulse sequences and parameters in order to understand how their selection affects image contrast. This brief review is intended to highlight common pulse sequences and parameters as well as introduce new techniques currently being released for clinical use.

MATERIALS
Basic pulse sequences are described and the influence of the acquisition parameters on image contrast are illustrated. Such basic sequences include the ubiquitous spin echo, fast spin echo, and gradient echo sequences. Specialized techniques for fat suppression and magnetic resonance angiography are also presented. Currently approved contrast agents for use in MRI are briefly reviewed, and various advanced pulse sequences, such as those for diffusion and magnetization transfer contrast imaging, are briefly outlined.

RESULTS
The utility of basic and advanced pulse sequences are demonstrated by clinical examples and images of normal brain and spine. New sequences and techniques are briefly outlined with regard to their potential for improving neuroimaging examinations.

CONCLUSIONS
This brief review outlines how the choice of pulse sequence and acquisition parameters influences the resulting image contrast for a variety of basic and advanced imaging techniques.

KEY WORDS
Magnetic resonance imaging, brain, review.

The soft tissue contrast provided by magnetic resonance imaging (MRI) has made it the modality of choice for imaging the central nervous system. The unchallenged sensitivity of MRI for the evaluation of central nervous system disease arises due to the dependence of MRI contrast and signal-to-noise ratio (SNR) on numerous intrinsic and extrinsic parameters. The most important intrinsic parameters, which depend upon individual tissue characteristics, include the spin–lattice relaxation time (T_1), spin–spin relaxation time (T_2), proton density, and velocity of moving protons. Extrinsic parameters affecting contrast and SNR are those chosen by the physician and/or technologist in performing the examination and include the echo time (TE), repetition time (TR), field-of-view, slice thickness, and resolution. In addition to the choice of these parameters, there is an almost bewildering choice of pulse sequences. A pulse sequence defines the manner in which the radiofrequency pulses, which generate the detectable signals, and magnetic gradient fields, which provide the spatial encoding of the signals, are applied. Fortunately, image contrast can be manipulated by both the choice of the extrinsic parameters and the selection of an appropriate pulse sequence to highlight regions of suspected pathology. Unfortunately, the large number of pulse sequences makes it difficult to comprehend the nuances of each pulse sequence. The purpose of this review is to briefly outline the most common pulse sequences and discuss the relative merits of each for neuroimaging. Despite the bewildering array of available pulse sequences, so many that a textbook exists simply to outline the types of sequences [39], the majority of

Address reprint requests to: Edward F. Jackson, Ph.D., Diagnostic Radiology, U. T. M. D. Anderson Cancer Center, 1515 Holcombe, Box 57, Houston, TX 77030.
Received April 18, 1996; accepted July 12, 1996.

0090-3019/97/$17.00
PII S0090-3019(96)00375-8

1 Image Contrast Using the Conventional Spin Echo Sequence

IMAGE CONTRAST WEIGHTING	TE	TR
T_1-weighted	Short (15–25)	Short (500–700)
T_2-weighted	Long (80–100)	Long (2500–3500)
Proton density-weighted	Short (15–25)	Long (2500–3500)

TE and TR are echo and repetition times, respectively. Values shown in parentheses are typical values in milliseconds.

current neuroimaging examinations employ only a few basic types.

BASIC PULSE SEQUENCES FOR MRI

SPIN ECHO PULSE SEQUENCE

Undoubtedly, the spin echo (SE) sequence is the most commonly utilized pulse sequence in neuroradiology. This section briefly outlines the key advantages of this sequence. More detailed descriptions of the SE sequence are given in several general MRI texts [15,17,28,58].

The SE sequence is characterized by two user selected delays, TE and TR. Briefly, the sequence consists of two radiofrequency pulses, the 90° pulse that creates the detectable magnetization, and the 180° pulse that refocuses it at the TE, and numerous magnetic field gradient pulses that encode frequency and phase to spatial location. The sequence is applied a number of times (typically 128–256) to uniquely encode the spatial locations. The TE is the time between the application of the 90° pulse, which creates the detectable magnetization, and the peak of the detected signal. The time between consecutive applications of the 90° pulse is the TR.

The choice of TE and TR determines whether the resulting image contrast depends upon the differences in T_1, T_2, or proton density among the tissues of interest. The resulting images are commonly termed T_1-weighted, T_2-weighted, and proton density-weighted, respectively. Table 1 outlines this dependence and gives typical values of TE and TR for the different weightings.

In T_1-weighted images (Figure 1**A**), tissues that have short T_1 relaxation times, particularly fat, appear bright; while those with long T_1 relaxation times, including fluids such as cysts, cerebrospinal fluid (CSF), and edema, appear dark. In T_2-weighted images (Figure 1**B**), tissues that have long T_2 relaxation times, such as fluids, appear bright. In the brain, differences in T_1 relaxation times between white matter and gray matter can allow for distinction of these tissues on heavily T_1-weighted images. In addition, the proton density of gray matter exceeds that of white matter by approximately 20% [61], thereby allowing clear depiction of white versus gray matter on proton density-weighted images (Figure 1**C**). In general, tissue signal intensities on proton density-weighted images mirror those obtained on T_2-weighted images. However, some white matter lesions, such as periventricular multiple sclerosis plaques, and some small superficial lesions, such as cortical strokes, are hyperintense relative to CSF on proton density-weighted images. Therefore, proton density-weighted images can aid in visualizing such lesions, which can be difficult to detect on T_2-weighted images alone because of the adjacent hyperintense CSF (Figure 2). Table 2 summarizes the appearance of various tissues and substances on T_1-weighted, T_2-weighted, and proton density-weighted images. In general, T_1-weighted images provide exquisite anatomic detail, while T_2-weighted images are generally superior for visualization of pathologic conditions.

FAST SPIN ECHO PULSE SEQUENCE

With the conventional SE pulse sequence, proton density-weighted and T_2-weighted images can take a significant amount of time to obtain (up to 10 minutes) because of the long TRs required. The fast spin echo (FSE) pulse sequence, based on the RARE technique proposed by Hennig et al. [24], allows for the acquisition of such images in a fraction of the time required by the conventional SE sequence. This is accomplished by uniquely phase-encoding a number of echoes during a given TR rather than just one echo as in the conventional SE sequence. The number of echoes phase-encoded in a given TR is frequently known as the echo-train length (ETL). For a given ETL, the theoretical reduction in scan time obtained by using FSE as compared to conventional SE is a factor of ETL, e.g., for an ETL of 8, the image can be acquired in one-eighth the time. The dramatic savings in time can be used to improve the SNR or the spatial resolution of the scans. There is, of course, a limit to how large the ETL can be without causing artifacts in the resulting image. This is particularly true for proton density-weighted or T_1-weighted images obtained with FSE when the use of large ETL values at short TEs can result in blurring and loss of contrast for small lesions with relatively short T_2 relaxation times [11]. Fortunately, this problem is basically nonexistent in T_2-weighted image acquisition, which is the

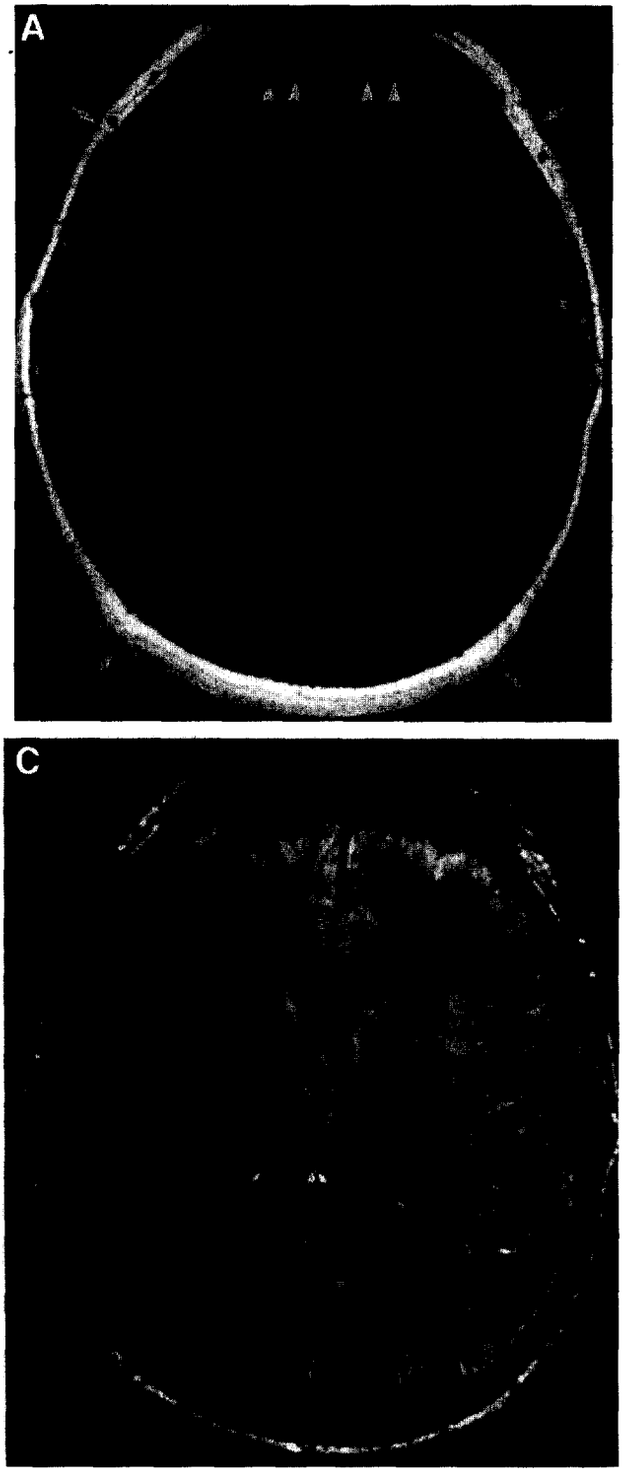

1 (**A**) T_1-weighted image, postgadolinium contrast enhancement; TE = 11 ms, TR = 500 ms. Note high signal intensity of subcutaneous fat (*arrows*) and low signal intensity of CSF and frontal sinus air (*arrowheads*); (**B**) T_2-weighted image; TE = 100 ms, TR = 3000 ms. Note how CSF is now bright and subcutaneous fat is of low intensity. Air remains a region of no signal intensity on all pulse sequences; (**C**) Proton density-weighted image, TE = 30 ms, TR = 3000 ms. CSF and fat are of intermediate signal intensity. Note the excellent differentiation between gray and white matter.

primary application of FSE, when using common values of ETL ranging from 8–16.

In general, T_2-weighted FSE image contrast is similar to that obtained with conventional SE for a given set of TE and TR values. In fact, upon quick viewing of T_2-weighted images, FSE and conventional SE sequences yield results that are indistinguishable. Upon closer evaluation, however, some notable differences become apparent [1,10,11,23, 37]. The most visually apparent difference is that fat is significantly brighter on T_2-weighted FSE sequences than on T_2-weighted conventional SE sequences using the same TE and TR values. Therefore, it is often necessary to use fat suppression

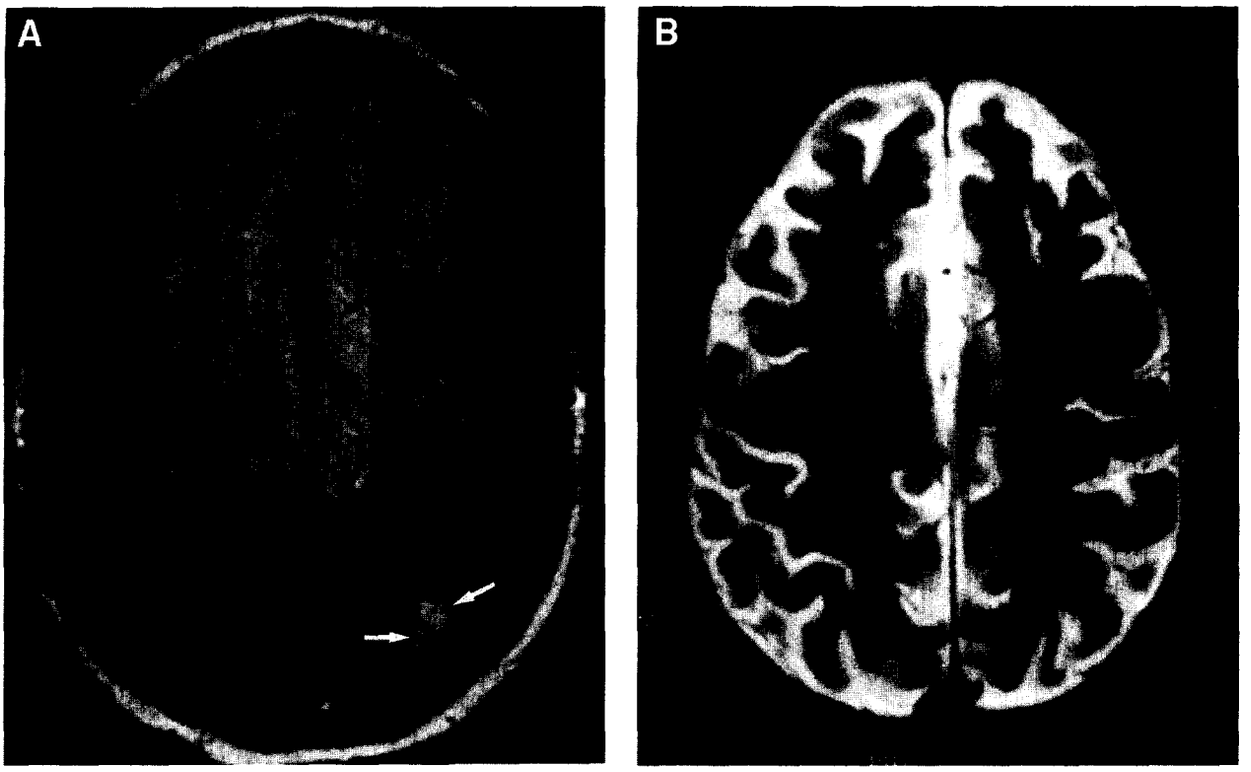

2 A seventy-five-year-old man with multiple small cortical infarcts. (**A**) Axial proton density-weighted image shows area of cortical hyperintensity representing infarction (*arrows*); (**B**) T_2-weighted image at the same level fails to reveal the lesion because of adjacent high signal intensity CSF.

techniques (discussed below). Furthermore, all FSE images demonstrate more T_2-weighting, regardless of TE and TR, making it difficult to obtain "true" proton density-weighted images. Finally, T_2-weighted FSE images demonstrate less loss of signal intensity from susceptibility changes caused by iron or deoxyhemoglobin. Therefore, areas that are hypointense on conventional T_2-weighted images

2 Appearance of Various Substances Relative to Cortex on T_1-Weighted, T_2-Weighted, and Proton Density-Weighted Spin Echo Images

Substance	T_1-Weighted	T_2-Weighted	Proton Density-Weighted
Fat and yellow marrow	+++	+	++
Proteinaceous material	++ (variable)	variable	variable
Intracellular methemoglobin	+++	–	–
Extracellular methemoglobin	+++	++	++
Deoxyhemoglobin	–	––	–
Hemosiderin	––	–––	––
Melanin	++	–	isointense
Calcium (some states)	+/–	–	–
Paramagnetic contrast agent	+++	minimal effect	minimal effect
Cyst	–	+++	++
Edema	–	+++	++
Vitreous humor	––	++	isointense
Cerebrospinal fluid	––	+++	isointense
Multiple sclerosis plaques	–	++	++
Tumors (most)	–	+ (complex)	+ (complex)
Abscess	–	+ (complex)	+ (complex)
Infarct	–	++	++
Iron (e.g., in globus pallidus)	––	–––	––
Air	no signal	no signal	no signal
Cortical bone	no signal	no signal	no signal

because of iron (e.g., globus pallidus and red nucleus) or deoxyhemoglobin are significantly less hypointense on T_2-weighted FSE images. This results in decreased image contrast for these tissues and in many institutions has limited the application of FSE sequences for routine intracranial T_2-weighted imaging. However, for high resolution T_2-weighted imaging (Figure 3**A**) and for routine T_2-weighted extracranial imaging, including the spine (Figure 3**B**) and neck [6,45], FSE has become a standard sequence.

GRADIENT-RECALLED ECHO PULSE SEQUENCES

Of all the pulse sequences used in MRI, the collection of sequences that fall under the general classification of gradient-recalled echo (GRE) sequences is the largest and has the most confusing list of names. This problem is only compounded by the fact that each manufacturer of clinical MR scanners has its own (lengthy) list of GRE sequences. Convenient sources of information for sorting through the "alphabet soup" of GRE sequences for different manufacturers are found in references 39 and 61.

In general, GRE sequences are significantly faster than SE sequences for obtaining proton density-weighted images, T_1-weighted images, and images similar to T_2-weighted images. Without going into a lengthy discussion of the physics of these sequences [57], the GRE sequences differ from the SE sequences because of the absence of the refocusing radiofrequency pulse (180° pulse). Furthermore, the single radiofrequency pulse in the GRE sequences is typically less than the 90° pulse used in SE sequences. This allows for a reduction in scan time, but at the price of SNR and increased artifacts due to changes in magnetic susceptibility between tissues. For example, at the interface of bone and tissue or air and tissue, there is a prominent loss of signal that gets worse as TE is increased. These artifacts, most noticeable at the skull base, generally preclude the use of GRE sequences for obtaining "T_2-like" image contrast. Furthermore, the advent of FSE sequences for fast T_2-weighted image acquisition has made the use of gradient echo sequences for obtaining T_2-like images nearly obsolete.

The speed of GRE sequences has made them the technique of choice for obtaining T_1-weighted images from a large number of slices or from a volume of tissue as opposed to slice-by-slice. GRE sequences, therefore, are frequently used for T_1-weighted three-dimensional (3D) volume data acquisition that may require 128 1–2 mm "slices." Such data can be reformatted to display the slices

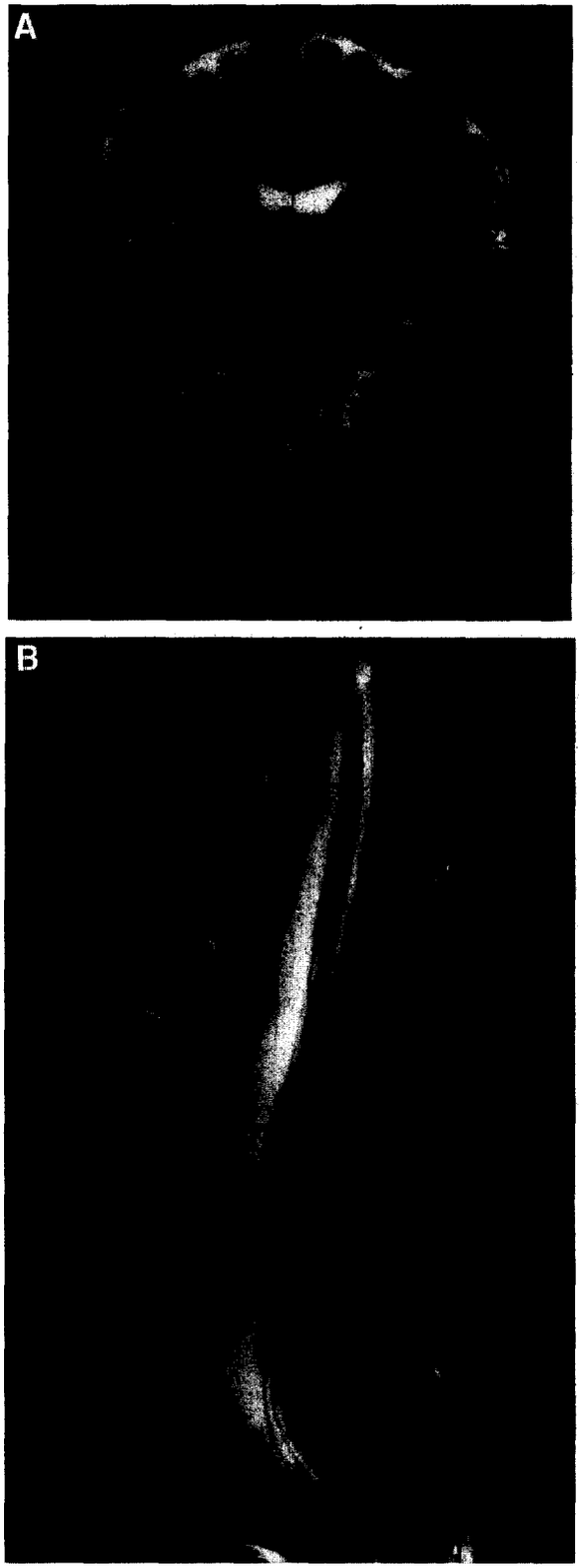

3 (**A**) High resolution coronal T_2-weighted FSE image of normal brain; TE_{eff} = 105 ms, TR = 5000 ms, ETL = 12; (**B**) sagittal T_2-weighted FSE image of the spine with fat suppression; TE_{eff} = 96 ms, TR = 3850 ms, ETL = 16. In addition to degenerative changes, multiple high signal intensity metastases can be seen within the vertebral bodies (*arrowheads*).

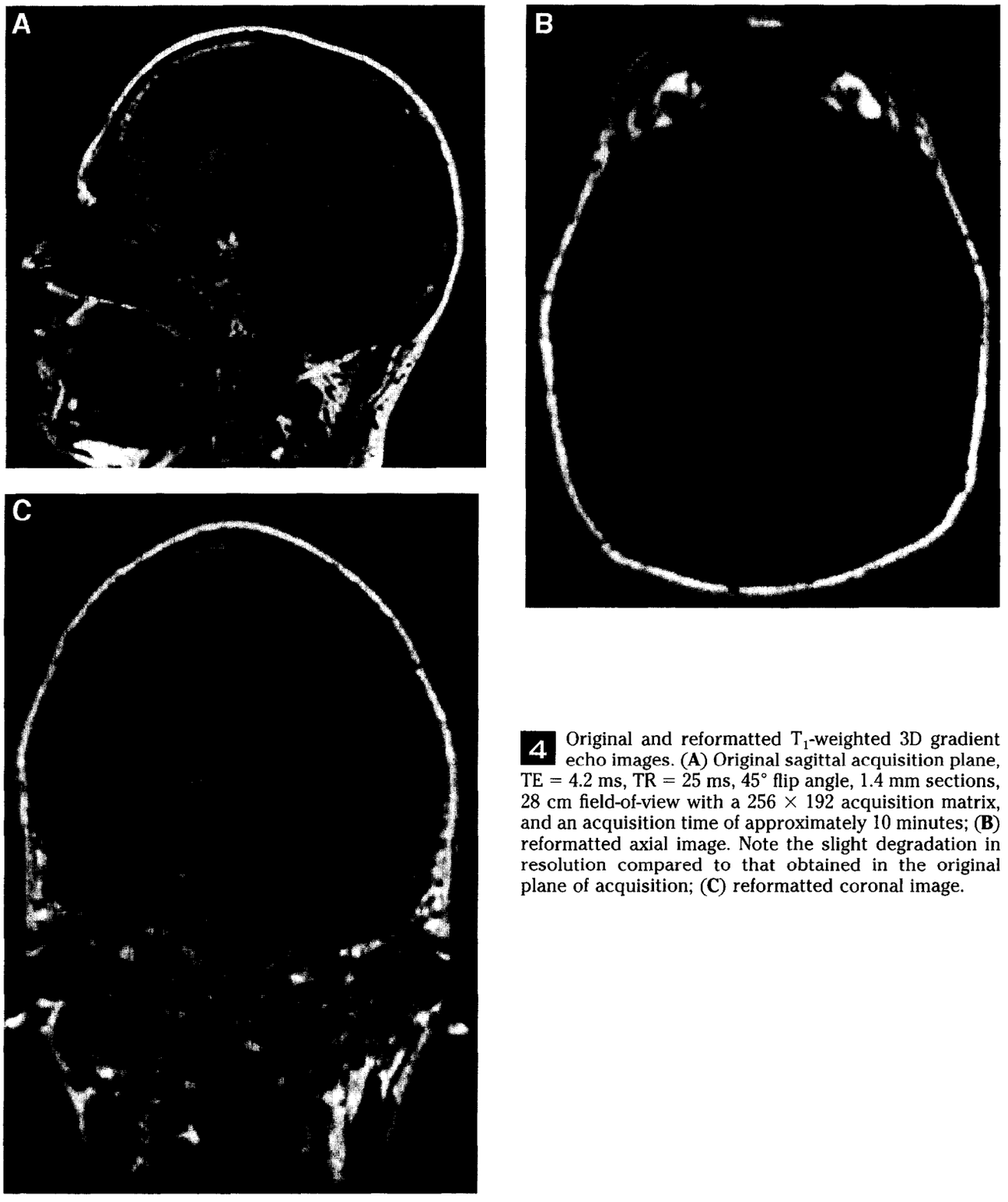

4 Original and reformatted T_1-weighted 3D gradient echo images. (**A**) Original sagittal acquisition plane, TE = 4.2 ms, TR = 25 ms, 45° flip angle, 1.4 mm sections, 28 cm field-of-view with a 256 × 192 acquisition matrix, and an acquisition time of approximately 10 minutes; (**B**) reformatted axial image. Note the slight degradation in resolution compared to that obtained in the original plane of acquisition; (**C**) reformatted coronal image.

in any plane such that data acquired with, for example, a sagittal prescription can be displayed in an axial, a coronal, or any oblique perspective (Figure 4). It must be realized, however, that the reformatted data will not have the same in-plane resolution as the original images unless the acquisition volume elements (voxels) are isotropic, i.e., the voxel dimensions are the same in all three directions. Typically, this is not the case because of image acquisition time constraints; therefore, the resolu-

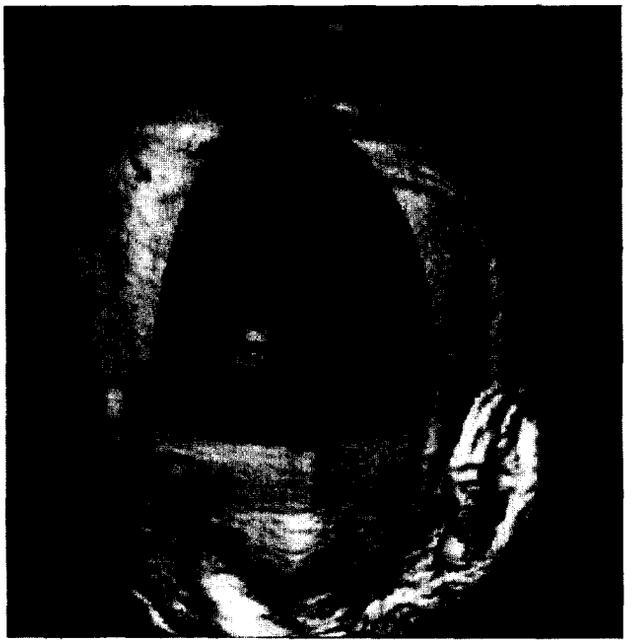

5 Surface rendered image from a postcontrast T_1-weighted 3D fast gradient echo acquisition; TE = 4.2 ms, TR = 15 ms, 25° flip angle. The enhancing metastatic lesion is seen in the cutaway view (*arrow*). The 3D rendering and cut-planes can be generated at any viewing angle.

6 A thirty-seven-year-old woman with a left optic nerve meningioma. Axial postcontrast fat-suppressed T_1-weighted image shows enhancement of the lesion surrounding the optic nerve (*arrowheads*). The orbital fat is suppressed, allowing visualization of the lesion as well as normal structures such as the extraocular muscles (*long arrows*) and lacrimal gland (*short arrow*).

tion in the reformatted images is inferior to the resolution in the original plane. Nevertheless, volume data have been rather extensively used to construct 3D rendered anatomic images for surgical planning (Figure 5) [4,9,26,56]. In addition, GRE sequences are used for all common forms of magnetic resonance angiography (MRA) (discussed below). This is due to: (1) the speed of the acquisition when acquiring the large amount of data required for MRA, (2) the decreased flow-related signal loss as compared to SE sequences resulting from the shorter TE times achievable with GRE sequences, and (3) the shorter TR times achievable with GRE sequences improves conspicuity of the vessels with respect to surrounding stationary tissues.

Using GRE sequences to routinely obtain postcontrast T_1-weighted images of the brain, while faster than using SE sequences, has not been widely accepted. One reason for this is the previously reported decreased lesion conspicuity on postcontrast GRE images as compared with SE images [7]. However, various types of magnetization-prepared GRE sequences have been proposed to decrease this deficiency [4,5].

Finally, continued improvements in MR hardware will allow for decreased minimum TE values, which will minimize the artifacts due to susceptibility changes discussed above as well as minimize flow-related signal loss in regions of turbulence, thereby improving MRA examinations.

FAT SUPPRESSION TECHNIQUES

It is often convenient to suppress the signal due to fat in order to more carefully examine the anatomy of interest (e.g., to better visualize enhancing lesions located adjacent to fat in the neck, orbits, or skull base) (Figure 6). This is particularly true on postcontrast T_1-weighted images or on T_2-weighted FSE images, where fat is brighter than on conventional SE sequences as outlined above. While inversion recovery techniques were initially commonly utilized, such techniques were generally quite time-consuming and inevitably yielded some suppression of water as well as fat, with a concomitant decrease in SNR. Currently, the most common method for fat suppression in MRI is the use of frequency-localized saturation pulses. The technique is commonly referred to as chemical saturation ("chem sat") or fat saturation ("fat sat"). In this case, saturation means the application of an additional 90° pulse that affects only the fat protons. This is possible because fat and water do not resonate at the same frequency; there is a separation of approximately 220 Hz at 1.5 T. This separation allows one to apply a 90° pulse only to the methyl and methylene lipid protons without affecting the water protons. The saturating 90° pulse ideally re-

sults in there being no detectable magnetization (i.e., signal, from the fat protons). Therefore, the fat is suppressed in the resulting image, while water is unaffected.

Although chemical saturation is the most widely utilized means of fat suppression, suboptimal suppression of fat can occur in any region of magnetic field inhomogeneity, such as regions of magnetic susceptibility changes found at air–tissue or bone–tissue interfaces. Such inhomogeneities may result in nonuniform suppression of fat across the image plane; this is more obvious in regions with abrupt changes in tissue types, such as the skull base and neck, or in large field-of-view imaging, such as thoracic spine examinations.

MRA PULSE SEQUENCES

One of the unique properties of MRI is that the signal intensity in the images is dependent on the velocity of the protons being imaged and, with the appropriate choice of pulse sequence, this dependence can be made the dominant factor. The key advantage of MRA lies in the fact that angiographic information can be obtained without the injection of an exogenous contrast agent. Different MRA techniques exist, and each has unique properties that are beyond the scope of this review. However, the basic strengths and advantages of the common sequences are outlined below. For more detailed discussions, an excellent text on MRA is available [42].

Two general pulse sequences are used in MRA: time-of-flight (TOF) techniques and phase-contrast (PC) techniques. TOF and PC data can be acquired in a two-dimensional (2D) or 3D fashion, each having its own advantages and disadvantages. In general, 2D techniques are better for slower flow and are capable of larger anatomic coverage as is required to image, for example, the internal carotid and vertebral arteries. However, for limited anatomic coverage of relatively fast flow, such as the circle of Willis, 3D techniques have a definite advantage in terms of resolution.

In TOF techniques, TE and TR values are both short, and one relies on the fact that during the time images are being acquired protons in the imaging plane are repeatedly being excited by the radiofrequency pulses without having time to completely relax (i.e., they become "partially saturated"). Because of this, protons in the image plane yield little signal. Protons in blood, on the other hand, continuously come into the slice and do not become saturated because they do not see repeated radiofrequency pulses. This flow-related enhancement produces greater signal from these moving protons than that obtained from surrounding stationary protons, allowing the visualization of vessels without administration of exogenous contrast agents. Because of their simplicity and speed, TOF sequences are currently the "workhorse" of MRA, particularly in neuroimaging. A typical high resolution MRA of the circle of Willis is given in Figure 7**A**, and a typical MRA of the internal carotid and vertebral arteries is given in Figure 7**B**.

In PC MRA techniques, one does not rely on the selective saturation of protons and the associated flow-related enhancement but instead takes advantage of the fact that moving protons have different phases than stationary protons have. In fact, the phase difference between moving and stationary protons is directly proportional to the velocity of the moving protons. This makes possible noninvasive measurements of the velocity and flow rate of blood using PC MRA [20,27,40,50]. Another key advantage of the PC technique is its sensitivity to slow flow as compared to TOF techniques. In fact, PC techniques have been utilized to image and measure extremely slow flow, such as CSF flow in aqueducts, in subarachnoid space, and in ventricular shunts [19,38]. Disadvantages of PC relative to TOF techniques include increased acquisition time and the necessity of specifying the maximum expected flow velocity before data acquisition begins.

In general, TOF techniques are preferred when imaging relatively rapid flow; while PC techniques are preferred when imaging very slow flow, or when quantitative flow information is desired. Both sequences will be greatly enhanced by newer, more powerful gradient systems that decrease the minimum TE that can be used. Short TEs are important in MRA because the signal intensity of moving protons is significantly decreased in regions of turbulent flow (e.g., at bifurcations or stenoses). This signal loss has frequently resulted in overestimation of stenosis based on MRA.

MR CONTRAST AGENTS

There are currently three MR contrast agents approved by the U.S. Food and Drug Administration [51]. All three are based on the paramagnetic properties of gadolinium, and they differ only in the ligands to which the gadolinium is associated. One of the three agents is ionic, while the remaining two are nonionic. The MR contrast agents do not cross an intact blood–brain barrier. In regions of blood–brain barrier breakdown, however, the agents

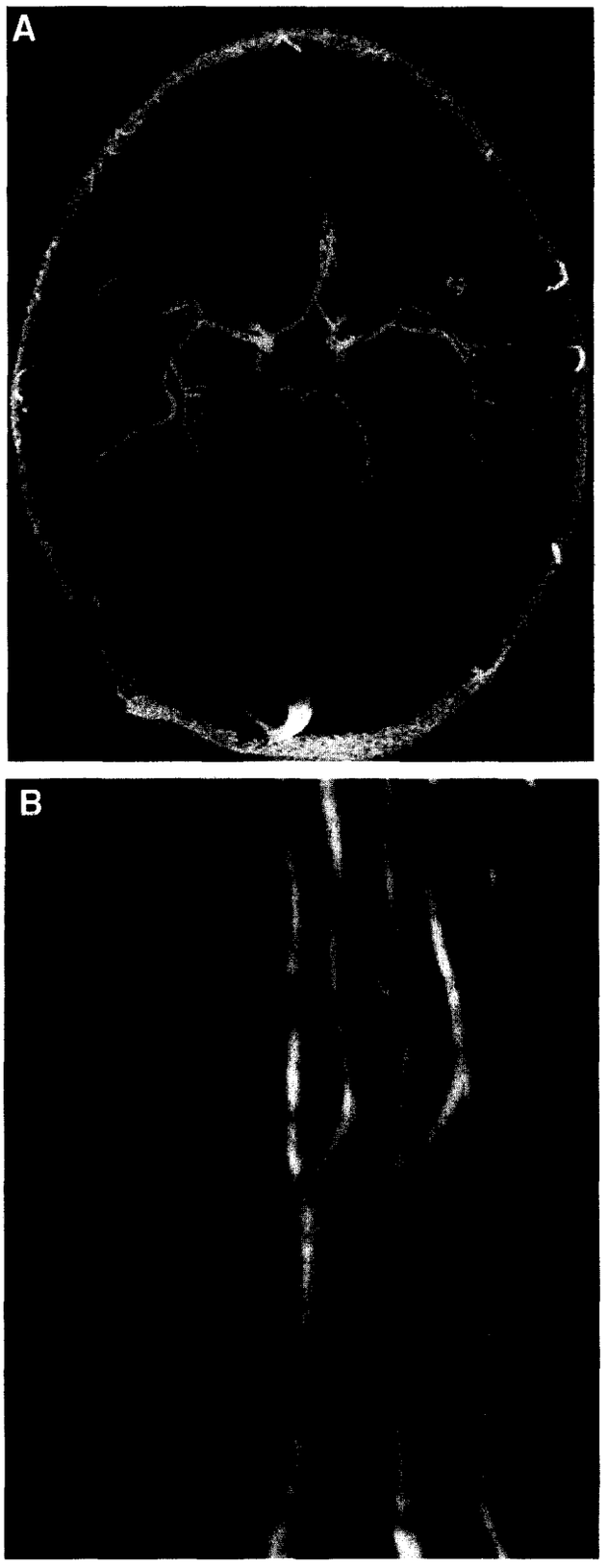

7 (**A**) High resolution 3D time-of-flight MR angiogram of the circle of Willis; (**B**) 2D time-of-flight MR angiogram of the internal carotid and vertebral arteries.

cause a local shortening of T_1 and T_2 relaxation times (preferential T_1-shortening occurs at the concentrations of gadolinium administered). Due to the shortened T_1 relaxation times, areas of blood–brain barrier breakdown enhance on T_1-weighted images, where tissues with short T_1 relaxation times appear hyperintense. Because of the improved conspicuity of lesions and the low risk associated with MR contrast agents, these agents are commonly used in intracranial MR examinations, particularly in brain tumor patients. Numerous additional contrast agents are currently in clinical trials, and it is expected that a large number of more specific agents will be in clinical use in the near future.

Advanced Pulse Sequences for MRI

The above pulse sequences and techniques form the foundation for routine clinical MRI. In the following sections, more recent additions to the MR armamentarium are outlined and applications of each are discussed. This section is meant to serve only as a brief synopsis of the various techniques. While a few are still in the research phase, it is anticipated that all will be commercially available in the near future.

Magnetization Transfer Contrast

A simple modification of the SE or GRE sequence (i.e., the addition of one additional radiofrequency pulse preceding the conventional sequence), adds a new mode of image contrast. In magnetization transfer (MT) contrast imaging, this MT pulse selectively saturates protons that have restricted motion, typically those associated with macromolecules such as proteins and membrane phospholipids [2,59,60]. Since protons bound to "free" water are in chemical exchange with the protons bound to the macromolecules, the magnetization is transferred from the macromolecular protons to the free water protons; therefore, in addition to T_1-weighting and T_2-weighting, image contrast also depends on the concentration of the macromolecules and the rate of exchange between the two pools of protons. MT pulses can be applied to any conventional imaging sequence. When used with T_1-weighted imaging, the primary visible effect is a decrease in white matter signal intensity relative to that of gray matter. This suppression of the white matter intensity frequently makes enhancing lesions more conspicuous on postcontrast T_1-weighted images (Figure 8). Therefore, MT tech-

8 (**Left**) T_1-weighted postcontrast image; TE = 15 ms, TR = 550 ms. (**Right**) T_1-weighted postcontrast image with magnetization transfer. Note the improved conspicuity of the lesions.

niques have frequently been used to improve the sensitivity of postcontrast T_1-weighted imaging of metastatic brain lesions, multiple sclerosis plaques, and other brain pathologies [3,18,21,25,34]. In addition, MT pulses have commonly been combined with TOF MRA sequences to greatly improve the contrast between vessels and brain parenchyma by suppressing the signal from the brain tissue and thereby increasing vessel conspicuity [14,32,41].

FLUID-ATTENUATED INVERSION RECOVERY PULSE SEQUENCES

Fluid-attenuated inversion recovery (FLAIR) sequences use an additional radiofrequency pulse applied at a carefully chosen time (the inversion time) prior to the conventional SE sequence. The amplitude of the pulse and the inversion time are chosen so that fluids such as CSF are strongly attenuated while the signal from brain parenchyma is only minimally affected. Therefore, this technique allows for the acquisition of images with T_2-contrast but with CSF and other low viscosity fluids suppressed [12,22].

Original applications of FLAIR were considerably time-intensive due to the long inversion times and TRs required to suppress fluids. Recent FLAIR techniques, based on FSE sequences, have made it possible to obtain 15–20 slices in less than 5 minutes and have expanded the use of FLAIR in neuroradiology [46,47].

A primary advantage of the FLAIR sequence is the improved conspicuity of periventricular lesions, such as multiple sclerosis plaques, or lesions adjacent to the sulci, such as infarcts (Figure 9). This technique may also be useful in the evaluation and follow-up of metastatic disease. Finally, FLAIR sequences have been combined with MT techniques to further improve the conspicuity of periventricular lesions.

DIFFUSION-WEIGHTED PULSE SEQUENCES

With appropriate gradient field pulses added during the echo time, a conventional SE sequence can be made to emphasize the effects of diffusion. In general, T_2-weighted images are acquired with and without the diffusion sensitizing gradients. In the diffusion-sensitized image, fluids that have freely diffusing spins are hypointense relative to their appearance on the nonsensitized image. In addition,

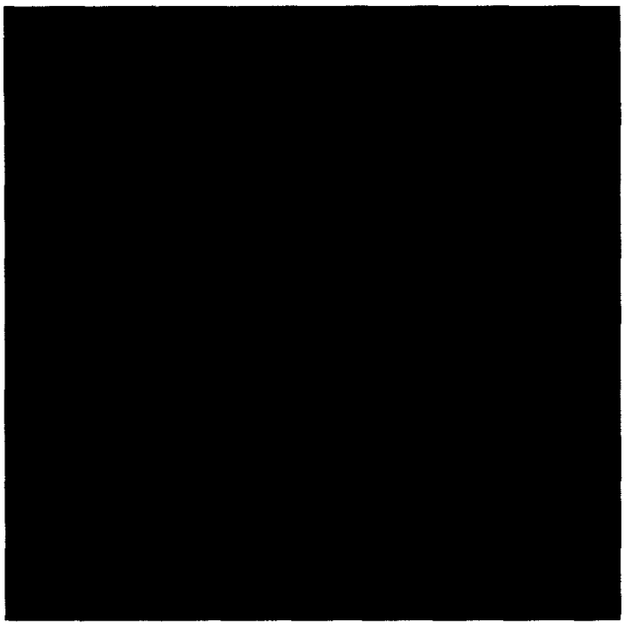

9 Axial fast FLAIR image (TE = 140ms, TR = 1200ms, TI = 2650ms) demonstrates hyperintense lesions in the anterior and posterior periventricular regions and the left basal ganglia. Smaller lesions are seen in the frontal white matter. The anterior periventricular lesions could not be seen on routine T2-weighted images. Note that although the signal intensity from the brain remains T2-weighted, the CSF is suppressed.

postprocessing of the images can generate an "apparent diffusion coefficient" image in which pixel intensity is directly proportional to the diffusion coefficient (i.e., regions of freely diffusing spins are hyperintense relative to regions where diffusion is restricted).

Clinical applications of diffusion-weighted images have included the separation of tumor core from other components such as edema, cysts, and necrosis [30,31,43] and in distinguishing cysts containing high levels of paramagnetic protein that would otherwise disguise their fluid-like nature. In addition, it has been shown that white matter tracts exhibit anisotropic diffusion (i.e., diffusion along the tracts is increased relative to diffusion across the tracts) [8,36]. Therefore, anisotropic diffusion-weighted imaging has been utilized to evaluate damage to white matter even before such damage is evident on routine MRI. Finally, since the diffusion coefficient is temperature dependent, diffusion-weighted imaging can be used for mapping temperature during hyperthermia due to radiofrequency or laser therapy [13,48,62].

Practically, diffusion-weighted imaging is quite challenging using currently available MR scanners because the diffusion effects are small compared with gross motion and, therefore, diffusion-weighted images may be highly susceptible to motion artifacts. This difficulty is being addressed by the improved gradient subsystems becoming available from a number of manufacturers.

ECHO PLANAR IMAGING PULSE SEQUENCES

One disadvantage of conventional MRI as compared to modalities such as computed tomography (CT) is the increased image acquisition time. The primary constraint on acquisition time, assuming sufficient SNR, has been the rate at which the magnetic field gradient coils can be switched. Research groups, and now MR system manufacturers, have developed gradient coils with greatly improved switching rates (more accurately slew rates). These coils have allowed for the implementation of pulse sequences, including the echo planar imaging (EPI) techniques, that are capable of obtaining an image in as little as 50 milliseconds. This capability has allowed for essentially real-time MRI, which has opened the door to novel applications of MR studies.

While the details of EPI are well beyond the scope of this review, the basic principle is similar to the FSE sequence described above, but to the extreme. In single-shot EPI, a single radiofrequency pulse is applied and all of the phase-encodings and frequency-encodings are done during one TR. In fact, for such a sequence TR is infinite. In general, T_1-weighted, T_2-weighted, and proton density-weighted images can all be acquired with minor modifications to the basic EPI sequence, and both SE-based and GRE-based EPI sequences exist.

Applications of EPI-type sequences have included ultrafast imaging to freeze cardiac and abdominal motion, imaging of uncooperative patients for whom severe motion artifacts preclude diagnostic studies with conventional sequences, improved diffusion-weighted imaging afforded by increased immunity to gross motion artifacts, relative cerebral blood volume (rCBV) mapping, and functional task-activation studies.

PERFUSION MRI PULSE SEQUENCES

Techniques for mapping rCBV have been proposed based on two basic principles. The first takes advantage of the transient susceptibility change that occurs when a bolus of paramagnetic contrast agent passes through the intracranial capillaries. The susceptibility change results in a transient decrease in signal intensity from brain tissue immediately surrounding the vessels. Therefore, areas of increased perfusion will appear hypointense relative to regions of decreased perfusion. Under the assumption that the contrast agent is intravascular

(no blood–brain barrier breakdown), such images can be used to construct maps of rCBV. Such studies have been used by groups at Massachusetts General Hospital, among others, to display the rCBV and to use this information to assist in the differentiation of tumor from radiation treatment effects [43]. This means of rCBV mapping requires EPI capability to acquire the images during the first pass of the contrast agent bolus. The SNR of these studies is quite acceptable, particularly if double-dose or triple-dose contrast agents are utilized.

The second means of evaluating perfusion, named EPISTAR (*e*cho-*p*lanar MR *i*maging and *s*ignal *t*argeting with *a*lternating *r*adiofrequency), uses a variation of the inversion recovery techniques and was first reported by Edelman et al. [16]. This technique actually requires no injection of contrast agent, but the SNR of the technique is typically inferior to the contrast-agent based methodology. As with the first technique, high speed imaging systems are necessary for good performance.

FUNCTIONAL MRI PULSE SEQUENCES

Recently, there has been significant interest in visualization of the centers of task activation using MRI. Two standard methods are utilized for such functional MRI and have been extensively reviewed by Kwong [29]. The first is based on the first pass bolus of contrast agent approach (outlined above) under the assumption that increased local blood flow resulting from task activation will yield increased susceptibility effects that can be used to highlight the centers of task activation. The advantage of this approach is good SNR of the resulting activation maps (up to 30% change in computed cerebral blood volume at 1.5 T) [44]. The disadvantage is the necessity of contrast agent administration, which limits repeated studies without the need for significant time delays between studies.

The second approach to functional MRI is known as BOLD (*b*lood *o*xygen *l*evel *d*ependent) contrast. In this technique, no contrast agent is administered, but high speed imaging hardware, although not necessarily required, is desirable [29]. The phenomenon that allows for detection of task activation centers in this method is the different magnetic properties of oxyhemoglobin and deoxyhemoglobin, the former being diamagnetic and the latter being paramagnetic. On task activation, the activation centers have an increased blood flow rate without an equal oxygen extraction rate, yielding a net increase in oxyhemoglobin as compared to deoxyhemoglobin. This difference gives rise to slight differences (approximately 2%–5% at 1.5 T) in image intensity on appropriately weighted MR images; these differences can be used to map the task activation. Although the SNR of the resulting maps is inferior to the bolus contrast agent approach, the BOLD technique has the advantage of being completely noninvasive, and repeated activation studies can be readily accomplished without significant time delays between activations. Also, the SNR of the BOLD maps is dependent on the magnetic field strength, with higher magnetic field strength resulting in increased SNR. Therefore, the availability of higher field strength magnets may increase the applications of BOLD techniques.

Recent uses of functional MRI have included mapping the task activation centers involved in photic stimulation, auditory stimulation, motor and sensory activation, and language activation. In addition, applications of these techniques to studies of visual processing and obsessive compulsive disorders have been reported [29].

Functional MRI has great potential for surgical planning by combining the mapping of such task activation centers with the exquisite anatomic data provided by MRI in the form of 3D surface or volume rendered data. The use of these data during surgery using probes interfaced with advanced image display workstations should provide a powerful tool for the planning and execution of neurosurgical procedures.

MRI-GUIDED THERAPY

With the advent of magnet designs that enable interventional MRI [33,52], the use of various combinations of pulse sequences for guiding neurosurgical procedures allows for an extremely powerful means of minimally invasive therapy. Without such "open magnets," the use of MRI to guide therapy has previously been centered around the use of MRI data to plan stereotactic procedures. Numerous factors influence the accuracy of MRI-based planning of such procedures [35,49,53–55]. Primary difficulties include: (1) nonlinearity of the magnetic gradient fields causing geometric distortions of the image (scanner-induced distortions), (2) geometric distortions resulting from magnetic field inhomogeneities due to the patient (object-induced distortions), and (3) chemical shift artifacts resulting in fat and water being slightly displaced from one another in the image even if they are actually in the same location. Additional difficulties may include flow-induced distortions (vessel-mismapping) and distortion of the magnetic field by the stereotactic frame itself [35]. The scanner-induced distortions

can be, and generally are, corrected by optimization of the magnetic field homogeneity by "shimming" and by postacquisition processing of the images using software from the MR system manufacturer. It is the object-induced distortions that typically limit the accuracy of MR-based stereoactic planning [35,53,54]. It is useful to note that the object-induced distortions and chemical shift artifacts both occur only in the frequency-encoding direction, not in the phase-encoding direction. Chemical shift artifacts can be minimized by using fat suppression techniques (discussed above). The object-induced distortions are complex, and correction algorithms are not widely available [55]. However, some choices of pulse sequence parameters can have a significant effect on geometric accuracy. In general, object-induced distortions decrease with decreasing field-of-view and/or increased sampling bandwidth. Typically, the largest errors due to object-induced distortions are at tissue–air and bone–tissue interfaces. Without correction, such distortions can be on the order of 2–3 mm. With careful choice of acquisition parameters and postacquisition software correction, accuracies of 1 mm and better can be obtained. As an alternative, some groups have used image fusion to overlay the MRI data on the more spatially accurate CT data.

While interventional MRI procedures are just becoming more readily available, the combined expertise of neurosurgeons, neuroradiologists, physicists, and engineers should soon make such powerful procedures feasible in routine clinical settings.

CONCLUSIONS

The goal of this review was to succinctly describe the current and research-level MRI pulse sequences and clinical applications of a wide range of techniques. It is hoped that this review will provide a starting point for wading through the "alphabet soup" of MR pulse sequences that are currently being routinely used as well as those that are making their way into clinical use.

REFERENCES

1. Atlas SW, Hackney DB, Listerud J. Fast spin-echo imaging of the brain and spine. Magn Reson Q 1993;9: 61–83.
2. Balaban RS, Ceckler TL. Magnetization transfer contrast in magnetic resonance imaging. Magn Reson Q 1992;8:116–37.
3. Boorstein JM, Wong KT, Grossman RI, Bolinger L, McGowan JC. Metastatic lesions of the brain: imaging with magnetization transfer. Radiology 1994;191:799–803.
4. Brant-Zawadzki MN, Gillan GD, Atkinson DJ, Edalatpour N, Jensen M. Three-dimensional MR imaging and display of intracranial disease: improvements with the MP-RAGE sequence and gadolinium. J Magn Reson Imaging 1993;3:656–62.
5. Brant-Zawadzki MN, Gillan GD, Nitz WR. MP RAGE: A three-dimensional, T_1-weighted, gradient-echo sequence—initial experience in the brain. Radiology 1992;182:769–75.
6. Chappell PM, Glover GH, Enzmann DR. Contrast on T_2-weighted images of the lumbar spine using fast spin-echo and gated conventional spin-echo sequences. Neuroradiology 1995;37:183–6.
7. Chappell PM, Pelc NJ, Foo TKF, Glover GH, Haros SP, Enzmann DR. Comparison of lesion enhancement on spin-echo and gradient-echo images. AJNR Am J Neuroradiol 1994;15:37–44.
8. Chenevert TL, Brunberg JA, Pipe JG. Anisotropic diffusion within human white matter: Demonstration with NMR techniques in vivo. Radiology 1990;177:401–5.
9. Cline HE, Lorensen WE, Souza SP, Jolesz FA, Kikinis R, Gerig G, Kennedy TE. 3D surface rendered MR images of the brain and its vasculature. J Comput Assist Tomogr 1991;15:344–51.
10. Constable RT, Anderson AW, Zhong J, Gore JC. Factors influencing contrast in fast spin-echo MR imaging. Magn Reson Imaging 1992;10:497–511.
11. Constable RT, Gore JC. The loss of small objects in variable TE imaging: implications for FSE, RARE, and EPI. Magn Reson Med 1992;28:9–24.
12. DeCoene B, Hajnal JV, Gatehouse P. MR of the brain using fluid-attenuated inversion recovery (FLAIR) pulse sequences. AJNR Am J Neuroradiol 1992;13: 1555–64.
13. Delannoy J, Chen C-N, Turner R, Levin RL, Le Bihan D. Noninvasive temperature imaging using diffusion MRI. Magn Reson Med 1991;19:333–9.
14. Edelman RR, Ahn SS, Chien D, Li W, Goldman A, Mantello M, Kramer J, Kleefield J. Improved time-of-flight MR angiography of the brain with magnetization transfer contrast. Radiology 1992;184:395–9.
15. Edelman RR, Kleefield J, Wentz KU, Atkinson DJ. Basic principles of magnetic resonance imaging. In: Edelman RR, Hesselink JR, eds. Clinical magnetic resonance imaging. Philadelphia: WB Saunders, 1990:3–38.
16. Edelman RR, Siewert B, Darby DG, Thangaraj V, Nobre AC, Mesulam MM, Warach S. Qualitative mapping of cerebral blood flow and functional localization with echo-planar MR imaging and signal targeting with alternating radio frequency. Radiology 1994;192:513–20.
17. Elster AD. Questions and answers in magnetic resonance imaging. St. Louis: Mosby, 1994.
18. Elster AD, King JC, Mathews VP, Hamilton CA. Cranial tissues: appearance at gadolinium-enhanced and nonenhanced MR imaging with magnetization transfer contrast. Radiology 1994;190:541–6.
19. Enzmann DR, Pelc NJ. Cerebrospinal fluid flow measured by phase-contrast cine MR. AJNR Am J Neuroradiol 1993;14:1301–7.
20. Enzmann DR, Ross MR, Marks MP, Pelc NJ. Blood flow in major cerebral arteries measured by phase-contrast cine MR. AJNR Am J Neuroradiol 1994;15:123–9.
21. Finelli DA, Hurst GC, Gullapali RP, Bellon EM. Im-

proved contrast of enhancing brain lesions on post-gadolinium, T_1-weighted spin-echo images with use of magnetization transfer. Radiology 1994;190:553–9.
22. Hajnal JV, DeCoene B, Lewis PD. High signal regions in normal white matter shown by heavily T_2-weighted CSF nulled IR sequences. J Comput Assist Tomogr 1992;16:506–13.
23. Henkelman RM, Hardy PA, Bishop JE, Poon CS, Plewes DB. Why fat is bright in RARE and fast spin-echo imaging. J Magn Reson Imaging 1992;2:533–40.
24. Hennig J, Nauerth A, Friedburg H. RARE imaging: a fast imaging method for clinical MR. Magn Reson Med 1986;3:823–33.
25. Hiehle JF, Grossman RI, Ramer KN, Gonzalez-Scarano F, Cohen JA. Magnetization transfer effects in MR-detected multiple sclerosis lesions: comparison with gadolinium-enhanced spin-echo images and nonenhanced T_1-weighted images. AJNR Am J Neuroradiol 1995;16:69–77.
26. Höhne KH, Fuchs H, Pizer SM. 3D imaging in medicine. Algorithms, systems, applications. New York: Springer-Verlag, 1990.
27. Jordan JE, Pelc NJ, Enzmann DR. Velocity and flow quantitation in the superior sagittal sinus with ungated and cine (gated) phase-contrast MR imaging. J Magn Reson Imaging 1994;4:25–28.
28. Kanal E, Wehrli FW. Signal-to-noise ratio, resolution, and contrast. In: Wehrli FW, Shaw D, Kneeland JB, eds. Biomedical magnetic resonance imaging. Principles, methodology, and applications. New York: VCH Publishers, 1988:47–114.
29. Kwong KK. Functional magnetic resonance imaging with echo planar imaging. Magn Reson Q 1995;11:1–20.
30. Le Bihan D. Clinical intravoxel incoherent motion imaging. In: Potchen EJ, Haacke EM, Siebert JE, Gottschalk A, eds. Magnetic resonance angiography. Concepts and applications. St. Louis: Mosby-Year Book, 1993:485–97.
31. Le Bihan D, Turner R, Douek P, Patronas N. Diffusion MR imaging: clinical applications. AJR Am J Roentgenol 1992;159:591–9.
32. Lin W, Tkach JA, Haacke EM, Masaryk TJ. Intracranial MR angiography: application of magnetization transfer contrast and fat saturation to short gradient-echo velocity-compensated sequences. Radiology 1993; 186:753–61.
33. Lufkin RB. Interventional MR imaging. Radiology 1995;197:16–8.
34. Mehta RC, Pike GB, Haros SP, Enzmann DR. Central nervous system tumor, infection, and infarction: detection with gadolinium-enhanced magnetization transfer MR imaging. Radiology 1995;195:41–46.
35. Michiels J, Bosmans H, Pelgrims P, Vandermeulen D, Gybels J, Marchal G, Suetens P. On the problem of geometric distortion in magnetic resonance images for stereotactic neurosurgery. Magn Reson Imaging 1994;12:749–65.
36. Moseley ME, Cohen Y, Kucharczyk J, Mintorovich J, Asgari HS, Wendland MF, Tsuruda J, Norman D. Diffusion-weighted MR imaging of anisotropic water diffusion in cat central nervous system. Radiology 1990;176:439–45.
37. Norbash AM, Glover GH, Enzmann DR. Intracerebral lesion contrast with spin-echo and fast spin-echo pulse sequences. Radiology 1992;185:661–5.
38. Norbash AM, Pelc NJ, Shimakawa A, Enzmann D. Shunt flow measurement and evaluation of valve oscillation with a spin-echo phase-contrast MR sequence. Radiology 1994;190:560–4.
39. Parikh AM. Magnetic resonance imaging techniques. New York: Elsevier, 1992.
40. Pelc NJ, Sommer FG, Li KCP, Brosnan TJ, Herfkens RJ, Enzmann DR. Quantitative magnetic resonance flow imaging. Magn Reson Q 1994;10:125–47.
41. Pike GB, Hu BS, Glover GH, Enzmann DR. Magnetization transfer time-of-flight magnetic resonance angiography. Magn Reson Med 1992;25:372–9.
42. Potchen EJ, Haacke EM, Siebert JE, Gottschalk A. Magnetic resonance angiography. St. Louis: Mosby, 1993.
43. Rosen BR, Aronen HJ, Cohen MS, Belliveau JW, Hamberg LM, Kwong KK, Fordham JA. Diffusion and perfusion fast scanning in brain tumors. In: Leeds NE, ed. Brain tumors. Philadelphia: WB Saunders, 1993:631–48.
44. Rosen BR, Belliveau JW, Aronen HJ, Kennedy D, Buchbinder BR, Fischman A, Gruber M, Glas J, Weisskoff RM, Cohen MS, Hochberg FH, Brady TJ. Susceptibility contrast imaging of cerebral blood volume: Human experience. Magn Reson Med 1991;22:293–9.
45. Ross MR, Schomer DF, Chappell P, Enzmann DR. MR imaging of head and neck tumors: comparison of T_1-weighted contrast-enhanced fat-suppressed images with conventional T_2-weighted and fast spin-echo T_2-weighted images. AJR Am J Roentgenol 1994; 163:173–8.
46. Rydberg JN, Hammond CA, Grimm RC, Erickson BJ, Jack CR, Huston J, Riederer SJ. Initial clinical experience in MR imaging of the brain with a fast fluid-attenuated inversion recovery pulse sequence. Radiology 1993;193:173–80.
47. Rydberg JN, Riederer SJ, Rydberg CH, Jack CR. Contrast optimization of fluid-attenuated inversion recovery (FLAIR) imaging. Magn Reson Med 1995;34:868–77.
48. Samulski TV, MacFall J, Zhang Y, Grant W, Charles C. Non-invasive thermometry using magnetic resonance diffusion imaging: potential for application in hyperthermic oncology. Int J Hyperthermia 1992;8:819–29.
49. Schad L, Lott S, Schmitt F, Strum V, Lorenz JW. Correction of spatial distortion in MR imaging: a prerequisite for accurate sterotaxy. J Comput Assist Tomogr 1987;11:499–505.
50. Schomer DF, Marks MP, Steinberg GK, Johnstone IM, Boothroyd DB, Ross MR, Pelc NJ, Enzmann DR. The anatomy of the posterior communicating artery as a risk factor for ischemic cerebral infarction. N Engl J Med 1994;330:1565–70.
51. Shellock FG, Kanal E. Magnetic resonance. Bioeffects, safety, and patient management. New York: Raven Press, 1994.
52. Silverman SG, Collick BD, Figueria MR, Khorasani R, Adams DF, Newman RW, Topulos GP, Jolesz FA. Interactive MR-guided biopsy in an open-configuration MR imaging system. Radiology 1995;197:175–81.
53. Sumanaweera TS, Adler JRJ, Napel S, Glover GH. Characterization of spatial distortion in magnetic resonance imaging and its implication for stereotactic surgery. Neurosurgery 1994;35:696–704.

54. Sumanaweera TS, Glover GH, Binford TO, Adler JR. MR susceptibility misregistration correction. IEEE Trans Med Imaging 1993;12:251–59.
55. Sumanaweera T, Glover G, Song S, Adler J, Napel S. Quantifying MRI geometric distortion in tissue. Magn Reson Med 1994;31:40–47.
56. Udupa JK, Herman GT. 3D imaging in medicine. Boca Raton: CRC Press, 1991.
57. Wehrli FW. Fast-scan magnetic resonance. Principles and applications. New York: Raven Press, 1991.
58. Wehrli FW, Haacke EM. Principles of MR imaging. In: Potchen EJ, Haacke EM, Siebert JE, Gottschalk A, eds. Magnetic resonance angiography. St. Louis: Mosby, 1993:9–34.
59. Wolff SD, Balaban RS. Magnetization transfer contrast (MTC) and tissue water proton relaxation in vivo. Magn Reson Med 1989;10:135–44.
60. Wolff SD, Eng J, Balaban RS. Magnetization transfer contrast: method for improving contrast in gradient-recalled-echo images. Radiology 1991;179:133–7.
61. Wood ML, Bronskill MJ, Mulkern RV, Santyr GE. Physical MR desktop data. J Magn Reson Imaging 1994; 3(S):19–26.
62. Zhang Y, Samulski TV, Joines WT, Mattiello J, Levin RL, Le Bihan D. On the accuracy on noninvasive thermometry using molecular diffusion magnetic resonance imaging. Int J Hyperthermia 1992;8:263–74.

COMMENTARY

This is well written and very clear for any physician's understanding. This is a very large subject, complex, and with unlimited variables. The authors have done a remarkable job of covering the subject in just 14 pages.

Glen D. Dobben, M.D.
Chicago, Illinois